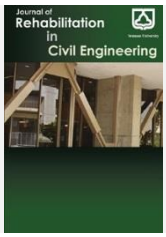

Journal of Rehabilitation in Civil Engineering

Journal homepage: https://civiljournal.semnan.ac.ir/

Biaxial Loading Capacity of H-Type Reinforced Concrete Electric Poles

Abolfazl Eslami [1,*]; Moein Ramezanpour [2]; Ehsan Hematpoury Farokhy [3]; Mohammad Dehghani Sanij [4]

1. Associate Professor, Department of Civil Engineering, Yazd University, Yazd, Iran
2. Research Associate, Department of Civil Engineering, Yazd University, Yazd, Iran
3. Ph.D. Candidate, Department of Civil Engineering, Yazd University, Yazd, Iran
4. Senior Engineer, Division of Engineering & Supervision, Yazd Electrical Distribution Company, Yazd, Iran
* Corresponding author: *a.eslami@yazd.ac.ir*

ARTICLE INFO

Article history:
Receive: 16 April 2023
Revise: 17 May 2023
Accept: 04 July 2023

Keywords:
H-type pole;
Reinforced concrete;
Loading capacity;
Biaxial bending
Interaction curve.

ABSTRACT

H-type reinforced concrete poles are nowadays widely used as an economical and cost-effective substitute for wooden poles in power transmission lines. Although these poles are frequently subjected to biaxial loading in real field application, their biaxial interaction curves yet await detailed investigation. The current study was aimed at developing the biaxial bending interaction curves for H-type utility poles considering the measurements stipulated by the relevant standards and codes. Towards this, two commonly used H-type electric poles (i.e., 9 and 12 m ones with a normal strength of 400 kgF) were constructed, cured, and loaded at angles of 0, 30, 60, and 90 degrees with respect to their minor principal axes. The experimental results were described in terms of load-displacement curves, developed strains, cracking pattern, failure modes, and biaxial loading interaction curve. The obtained interaction diagrams can be reliably used to estimate the loading capacity of electric poles under biaxial loading in real field applications.

E-ISSN: 2345-4423

How to cite this article:
Eslami, A., Ramezanpour, M., Hematpoury Farokhy, E., & Dehghani Sanij, M. (2024). Biaxial loading capacity of H-type reinforced concrete electric poles. Journal of Rehabilitation in Civil Engineering, 12(1), 63-76. https://doi.org/10.22075/jrce.2023.30322.1835

1. Introduction

Poles are structural elements that support overhead cables distributing electric power or other public utilities [1]. For many years, wooden and steel poles have been used in power distribution and transmission lines. Nowadays, however, the widespread use of wooden poles in utility lines is declining due to environmental concerns and durability problems [2]. On the other hand, application of steel poles is limited due to high production costs and few available production facilities [3]. Consequently, utility companies are encouraged to consider concrete poles as the most cost-effective and predominant support for power lines [4]. Compared to their pre-stressed counterparts, non-prestressed H-type concrete poles are very common in Iran owing to their lower construction cost and abundance of manufacturing plants [5].

Despite several research studies on the loading capacity of concrete columns including concrete filled steel tubular sections [6,7], a few have so far focused on the loading capacity and failure modes of concrete poles used in power distribution lines. Henin et al. [8] reported that failure of their tested concrete poles was accompanied by yielding of longitudinal bars in the tension zone near the ground level at the position of maximum flexural moment followed by concrete crushing in the compression zone. Vivek et al. [9] subjected tapered concrete poles embedded in various footings to monotonic loading and unloading sequences to determine their ultimate capacity. Based on their results, failure was accompanied by narrow transverse cracks on the tension side of the section. Kilukas et al. [10] investigated the performance of concrete poles that had been in service in power distribution lines for more than 30 years and sustained different types of deterioration. In another experimental study, Kilukas et al. [11] examined the deteriorated concrete poles to find that their collapse was mainly caused by the failure of longitudinal reinforcement. Argo [12] investigated the load bearing capacity of full-scale H-type concrete poles under monotonic loading. The observed cracks mainly developed in the maximum bending moment zone before they further propagated to the longitudinal reinforcement and that the pole collapse was primarily accompanied by concrete spalling in the compression zone. Baghmisheh and Mahsuli [13] experimentally validated finite element models to estimate the seismic behavior of concrete H-type electric poles. The study was focused on the effects of loading patterns in seismic performance of H-type concrete poles of two different lengths of 9 and 12 m. It was found that the vulnerability of the modeled H-type concrete poles would increase with their length.

Zeynalian and Khorasgani [14] subjected three full-scale H-type concrete poles, 12 m in length, to a loading regime that met the criteria stipulated by the Iranian Standard for H-type Utility Poles [15] and find that all the pole specimens offered similar loading capacities. Their results were then used to develop a nonlinear finite element model.

Despite the widespread use of H-type non-prestressed concrete poles in power distribution lines, no detailed study was reported on their structural behavior under biaxial bending moments. This is of particular importance since such structural members are frequently subjected to biaxial loads in most real field applications. To fill this knowledge gap, the current experimental study was implemented to evaluate the structural performance of H-type electric poles under biaxial loading. As the case study, two commonly used electric poles (i.e., 9 and 12 m H-type concrete poles with a nominal loading capacity of 400 kgF) were cast for careful examination under such loads. In addition, the relevant biaxial loading capacity interaction curves were drawn by conservative estimation of the actual curves using a three linear diagram.

2. Experimental program

2.1. Material properties

All the pole specimens were fabricated and cast in a single day to achieve a target 28-day compressive strength of at least 30 MPa as required by the Iranian Standard for H-type Utility Poles [15]. Table 1 reports the mix proportion of the concrete. During casting, nine cylindrical specimens (150mm×300mm) were prepared from the same batch used for constructing the poles to determine the concrete compressive and tensile strengths (Table 2). The mechanical properties of the steel reinforcement as determined based on ASTM A615 [16] are also reported in Table 3.

Table 1. Concrete mix proportions.

	Cement ($\frac{kg}{m^3}$)	Fine sand ($\frac{kg}{m^3}$)	Gravel ($\frac{kg}{m^3}$)	Water (lit)	$\frac{w}{c}$
Quantity	400	950	775	205	0.54

Table 2. Mechanical properties of concrete.

	Compressive strength (MPa)	Tensile strength (MPa)
Average 7-day value	24.7	-
Average 28-day value	31.8	3.5

Table 3. Mechanical properties of steel reinforcement.

Type	Diameter (mm)	Surface shape	Tensile strength (MPa)	Elastic modulus (GPa)
Transverse rebars	6	Smooth	352	204
Longitudinal rebars	14 and 16	Deformed	621	201

2.2. Specifications of the test specimens

In this study, H-type concrete poles of 9 and 12 m in length with a normal loading capacity of 400 kgF were selected as they are the most commonly used in electricity distribution lines in Iran. Fig. 1 presents the geometric and reinforcement details of the poles. All the transverse reinforcements were made of 6 mm smooth rebars while the longitudinal bars were from deformed bars of 14 and 16 mm in diameter. To achieve reliable results with a minimum number of the test specimens, the biaxial loading capacity interaction curve was estimated, albeit conservatively, by a three linear diagram drawn using four points. Each point belongs to the biaxial loading capacity of a pole at a specific angle, θ, (i.e., 0, 30, 60, or 90 degrees) relative to the X-axis (minor principal axis) as shown schematically in Fig. 2. For each point, the average value obtained from testing two specimens (one original and one replicate specimen) was considered as the corresponding strength. This yielded a total number of 16 H-type concrete poles.

The test specimens were designated with an initial number referring to the pole height (i.e., 9 or 12 m) followed by its normal loading capacity. In addition, the third number represented the loading angle (i.e., 0, 30, 60, or 90 degrees) while the last one indicated the number of replicate specimen. For example, 9-400-0-1 refers to the first 9 m pole with a normal capacity of 400 kgF loaded at an angle of zero.

2.3. Test setup, instrumentation, and loading

The loading setup was similar to that proposed by the Iranian Standard for H-type Utility Poles [15], as shown schematically in Fig. 3 for the loading angle of zero. Accordingly, the restraint length of each pole was 14% of its total length (1260 and 1680 mm for the 9 and 12 m poles, respectively).

The specimens were fixed on the support using three hydraulic jacks while the load would be applied monotonically through a wire rope puller at a distance of 600 mm from the pole tip. Necessary adjustments were made to test pole specimens under other angles. Fig. 4 shows the 9 m concrete poles under all the loading angles. During the test, load variations would be measured using a 50 kN load cell with an accuracy of ±0.04 kN while

displacement fluctuations at the loading point would be monitored through a laser meter possessing an accuracy of ±1 mm. Moreover, variations in the strain values of concrete and steel reinforcement would be traced using strain gauges installed 300 mm away from the support in the 9-400 poles that had been loaded to bend about their major principal axes (i.e., 9-400-0-1 and 9-400-0-2). During the tests, variations in load and strain values were recorded using a data acquisition system.

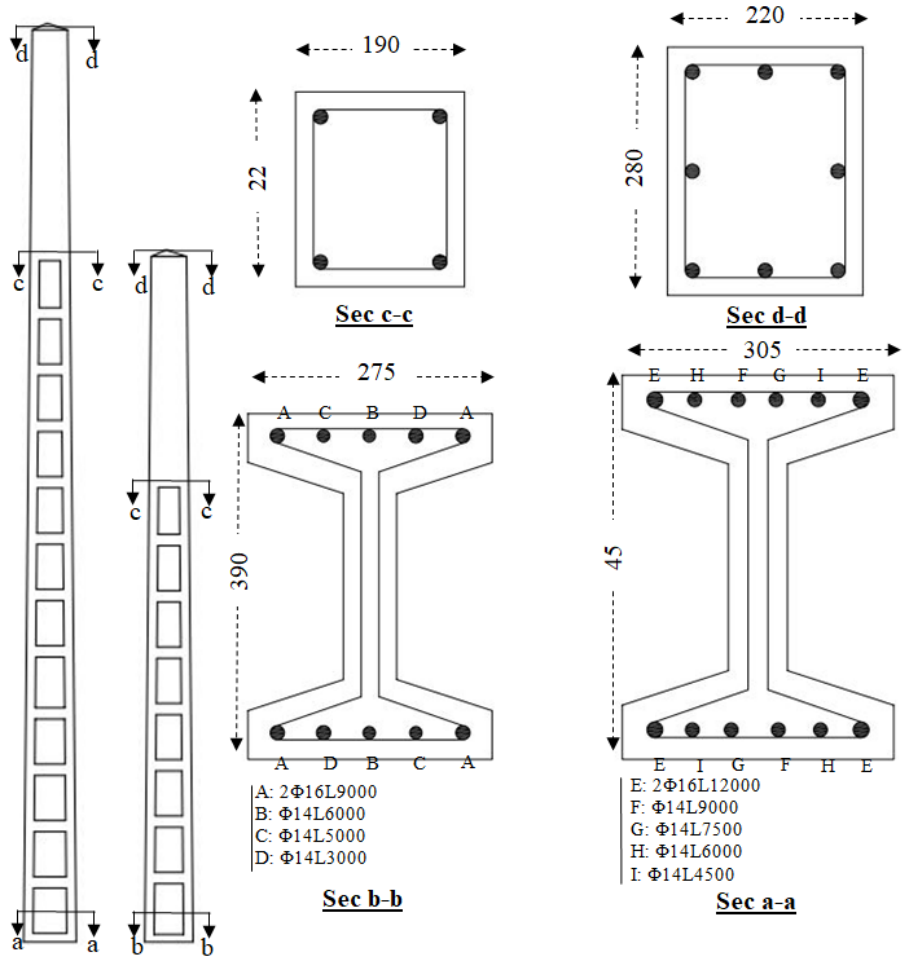

Fig. 1. Geometry and reinforcing details of the test specimens (dimensions are in mm).

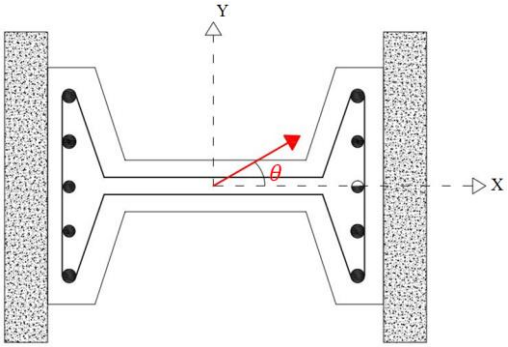

Fig. 2. Pole section with the loading angle (θ) relative to the X-axis.

The tests were carried out under either of two loading regimes. The first one was proposed by the Iranian Standard for H-type Utility Poles [15] as shown in Fig. 5 while the second loading regime was a monotonically increasing load up to failure. These loading regimes were aimed at bending the H-type electric poles about their major principal axes in order to realize their structural performance at normal (design), elastic, and ultimate strengths.

Normal (design) strength is defined as the maximum loading capacity of a pole under field conditions while the elastic one is higher by 50%. Ultimate strength should be at least 3.0 or 2.5 times the normal strength for the normal capacity of up to 400 kgF or higher values, respectively. Ultimate strength is that at which no remarkable increase is observed in load while displacement rises unless the pole

fails earlier. In other words, the post-yield behavior of the poles is ignored and the obtained interaction curve is the yield biaxial bending moment interaction curve. Table 4 summarizes the compulsory acceptance loading thresholds as stipulated by the Iranian Standard for H-type Utility Poles [15]. Throughout the loading process, the poles were visually inspected to detect cracks and failures.

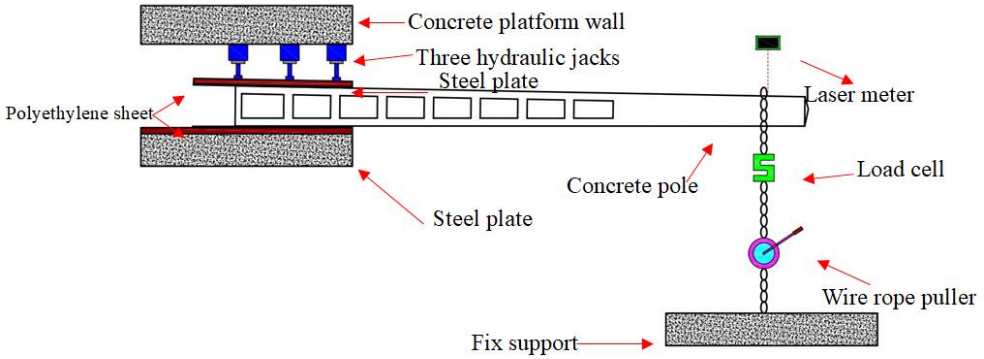

Fig. 3. Test setup and instrumentation.

(a) zero degree

(b) 30 degree

(c) 60 degree

(d) 90 degree

Fig. 4. The 9-400 poles tested at four rotation angles.

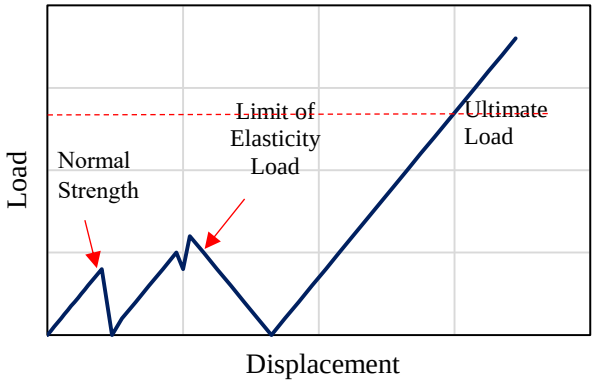

Fig. 5. Schematic illustration of the loading protocol proposed in the Iranian Standard for H-type Utility Poles.

Table 4. Minimum required resistance of 9-400 and 12-400 poles according to the Iranian Standard [15].

Type of specimen	Height (m)	Normal strength load (kgF)	Limit of elasticity load (kgF)	Ultimate strength load (kgF)
9-400	9	400	600	1200
12-400	12	400	600	1200

3. Experimental results and discussion

3.1. Load-displacement responses

As mentioned, the pole specimens were subjected to two loading protocols at the angle of zero degree (i.e., 9-400-0-1 and 12-400-0-1) for comparison purposes.

Fig. 6 provides the variations in load versus the corresponding displacement for 9-400-0-1 and 12-400-0-1 under the first loading protocol proposed by the Iranian Standard for H-type Utility Poles [15]. Fig. 7 compares the load-displacement behavior of the poles at the angle of zero under both loading regimes. For ease of comparison, the unloading parts were eliminated for the specimens tested under the first loading protocol. Clearly, the load-displacement responses under the selected loading histories are almost identical. Thus, they are used interchangeably in this study. Further, the ultimate loading capacities of both poles loaded to bend about their major principal axis (at the angle of zero) were much higher than the threshold (1200 kgF) stipulated by the Iranian Standard for H-type Utility Poles [15] with 400 kgF normal strength. It should be noted that the plateau in the load-displacement curve of 12-400-0-2 outlines the yielding of longitudinal steel reinforcement during loading as evidence by the test observations. This yielding part should be ignored according to the Iranian Standard [15].

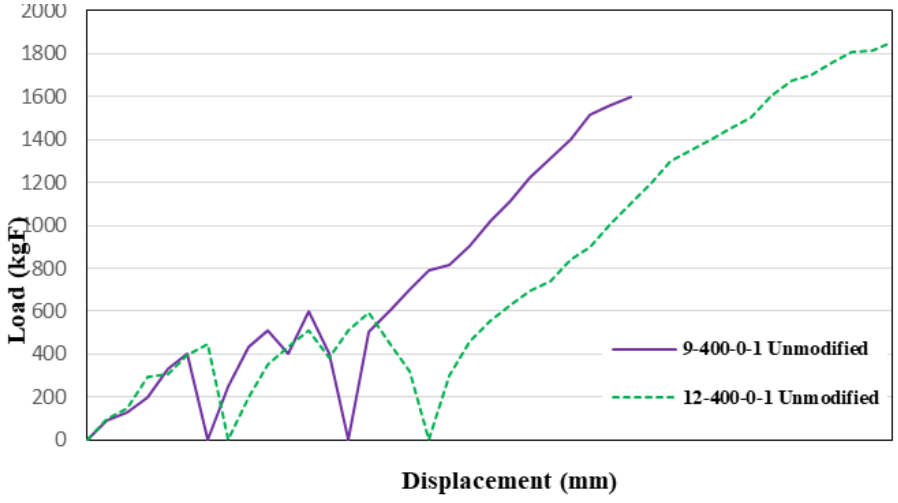

Fig. 6. Load-displacement curves of the poles tested at the angle of zero under the first loading regime.

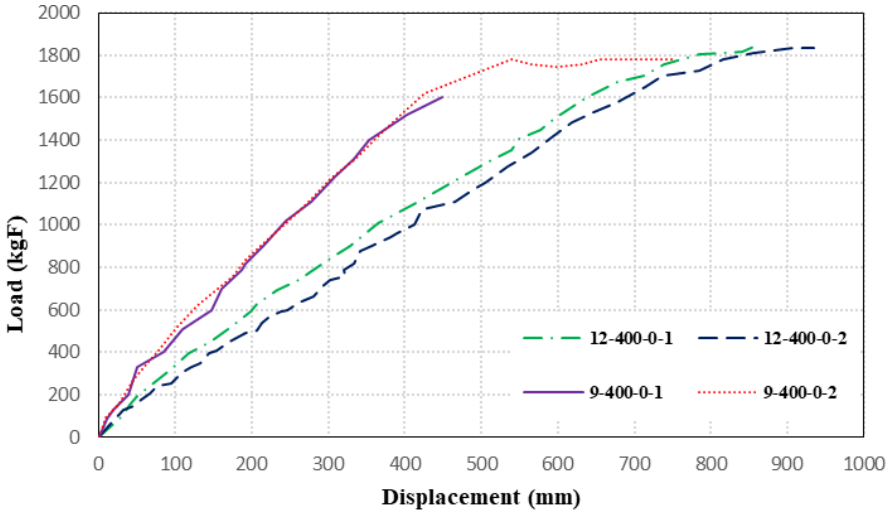

Fig. 7. Comparison of the load-displacement curves of the poles subjected to the two loading regimes at the angle of zero.

Except for the poles loaded at zero degree, all the others were tested under the first loading regime (i.e. monotonically increasing the load) up to failure. Fig. 8 compares the load-displacement curves for all the tested poles at different angles. Based on the obtained results, the load-displacement behavior of the poles loaded at 60° is close to those bent about their minor principal axes (90°) while those loaded at 30° are similar to those bent about their major principal axes (zero degree).

Tables 5 and 6 provide numerical comparisons of the maximum load carrying capacities, P_{max} (as per the Iranian Standard [15]), their differences from those obtained for specimens loaded to bend about the major principal axes (at zero angle), and the failure modes observed in all the tested poles. As expected, the loading capacity of poles decreased with increasing loading angle relative to the minor principal axis. The average load carrying capacities of the poles tested at 30° were around 3 and 11% lower than those obtained for 9-400 and 12-400 at zero angle, respectively. At 60°; however, the strength reductions of 29 and 39% were observed in 9-400 and 12-400, respectively. Moreover, the loading capacities of 9-400 and 12-400 specimen bend about their minor principal axes (90°) were reduced by 33 and 43%, respectively, compared to those bent about their major principal axes (zero degree).

The common failure modes observed in the concrete poles included shear failure (SF) at the test support, flexural failure (FF), or their combination. Shear failure can be primarily described with diagonal cracks at support while flexural failure is accompanied by cracks perpendicular to the pole at the web and flange mainly near the support point.

Table 5. Summary of the test results and failure modes of the 9-400 poles.

Specimen	Rotation angle (θ)	P_{max} (kgF)	P_{Ave} (kgF)	Difference# (%)	Failure mode
9-400-0-1	0	1601	1691.5	-	SF
9-400-0-2	0	1782			
9-400-30-1	30	1643	1634.5	-3	SF-FF
9-400-30-2	30	1626			
9-400-60-1	60	1190	1197.5	-29	SF-FF
9-400-60-2	60	1205			
9-400-90-2	90	1204	1133	-33	FF
9-400-90-1	90	1062			

Note: SF = shear Failure; FF = Flexural Failure;
Average difference of P_{Ave} relative to that at zero angle.

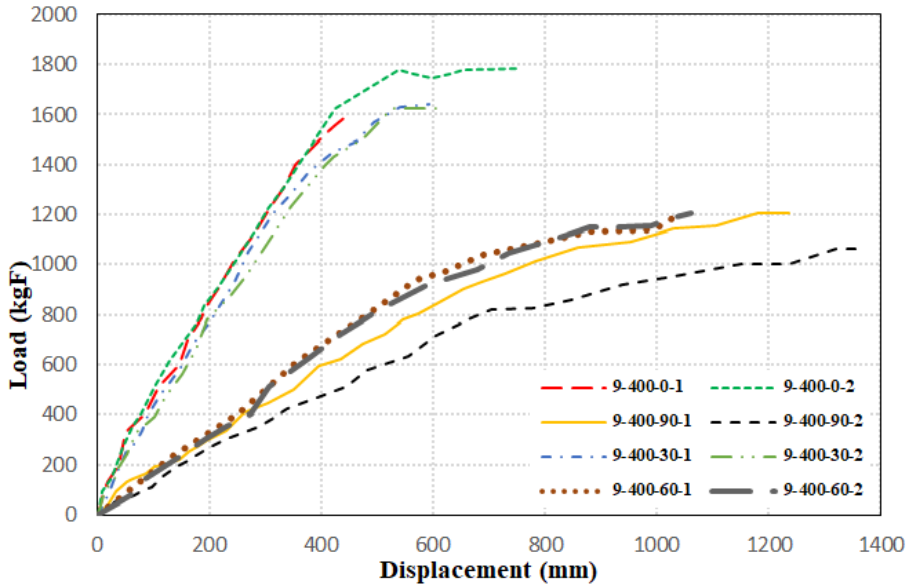

(a) 9-400 poles

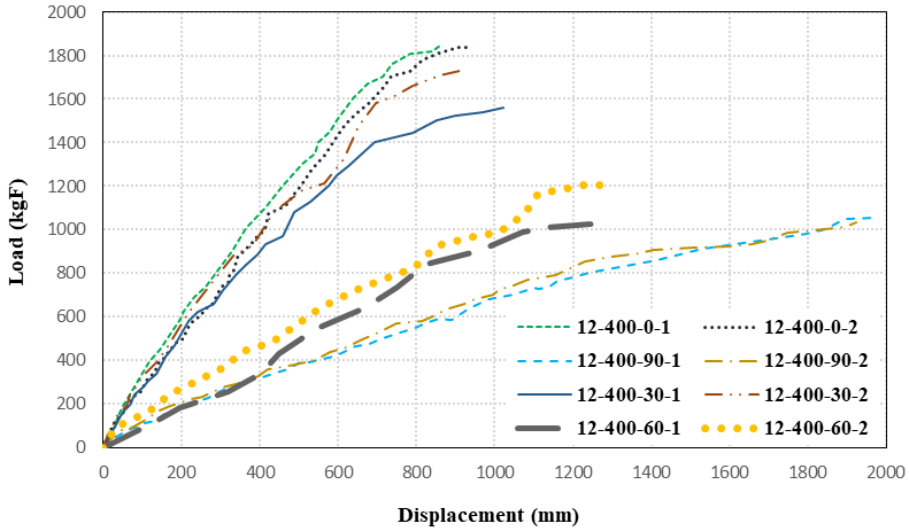

(b)12-400 poles

Fig. 8. Load-deflection curves of a) 9-400 and b) 12-400 specimens.

Table 6. Summary of the test results and failure modes of the 12-400 poles.

Specimen	Rotation angle (θ)	P_{max} (kgF)	P_{Ave} (kgF)	Difference# (%)	Failure mode
12-400-0-1	0	1850	1843	-	SF
12-400-0-2	0	1836			
12-400-30-1	30	1563	1649	-11	SF-FF
12-400-30-2	30	1735			
12-400-60-1	60	1026	1116	-39	SF-FF
12-400-60-2	60	1206			
12-400-90-2	90	1056	1044.5	-43	FF
12-400-90-1	90	1033			

Note: SF = shear Failure; FF = Flexural Failure;
Average difference of P_{Ave} relative to that of zero angle.

3.2. General behavior and observation

3.2.1. Poles loaded at 0°

At this angle, the poles are loaded to bent about their major principal axis. This is the loading direction necessitated by the Iranian Standard for H-type Utility Poles for structural health monitoring of poles [15]. Towards this, 9-400-0-1 and 12-400-0-1 were loaded accordingly (loading regime 1) while 9-400-0-2 and 12-400-0-2 were subjected to a

monotonically increasing load (loading regime 2). The first noticeable cracks in 9-400-0-1 were observed at the second step restricted within the base at a load of 401 kgF corresponding to a displacement of 84 mm. In 9-400-0-2, cracks initiated at the same place and similar load corresponding to a displacement of 77 mm. As loading proceeded, flexural cracks propagated along the length of the poles. Subsequently, diagonal shear cracks also appeared in the first two steps of the poles at the support leading to ultimate failure as shown in Fig. 9. The maximum recorded loading capacities were 1601 and 1780 kgF for 9-400-0-1 and 9-400-02, respectively.

The first visible cracks in 12-400-0-1 and 12-400-0-2 developed at the first two steps within the base and at loads of 397 and 393 kgF corresponding to displacements of 117 and 144 mm, respectively. With the load increment, diagonal cracks expanded at the support leading to the ultimate failure at loads of 1850 kgF for 12-400-0-1 and 1836 kgF for 12-400-0-2. Fig. 10 shows the shear cracks and failure status in both 12-400-0-1 and 12-400-0-2. The formation of shear cracks inside the support may be attributed to the high shear force arising from the three concentrated reactions. Such behavior can hardly ever happen in real field conditions due to the continuous support provided by the surrounding concrete foundation and the soil. Consequently, it is estimated that the loading capacity of poles in real field conditions might be higher than that achieved through the implemented setup which is proposed by the Iranian Standard for H-type Utility Poles [15].

(a) (b)

Fig. 9. Diagonal shear cracking of: a) 9-400-0-1, and b) 9-400-0-2.

(a) (b)

Fig. 10. Shear cracks in: a) 12-400-0-1, and b) 12-400-0-2.

3.2.2. Poles loaded at 30°

Four poles (namely, two 9-400 and the two 12-400 specimens) were subjected to a monotonically increasing load up to failure at this angle (i.e., the second loading regime). The initial responses observed in 9-400-30-1 and 9-400-30-2 loaded at 30° relative to the minor principal axis involved flexural cracks at their flange at loads of 159 and 242 kgF, respectively. This was followed by new flexural cracks at loads of 260 and 393 kgF while both specimens exhibited diagonal shear cracks at their support at a higher load of 650 kgF. The maximum loads carried by 9-400-30-1 and 9-400-30-2 were measured to be 1643 and 1626 kgF, respectively. These two poles finally failed due to a combination of shear and flexural cracks as indicated in Fig. 11.

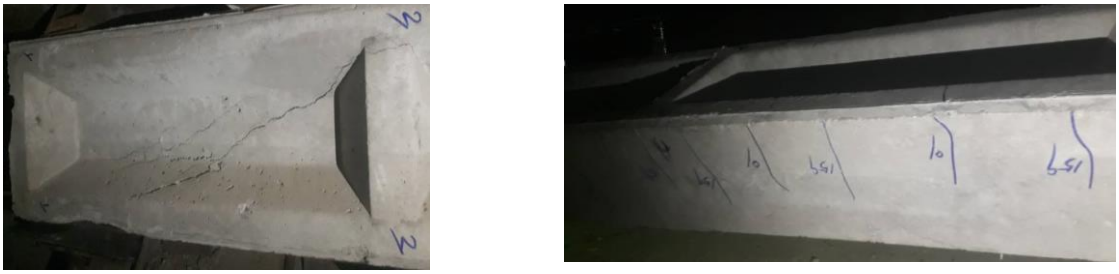

(a)

(b)

Fig. 11. Cracking in: a) 9-400-30-1, and b) 9-400-30-2.

The first flexural cracks in 12-400-30-1 and 12-400-30-2 were observed at loads of 215 and 209 kgF, respectively, followed by diagonal cracks at the two restricted steps at a load of 650 kgF. The maximum load carrying capacity of 12-400-30-1 was 1563 kgF while 12-400-30-2 could bear 1735 kgF. According to Fig. 12, combined shear and flexural cracks clearly have led to failure of 12-400-30-1 and 12-400-30-2.

(a)

(b)

Fig. 12. Cracking status in: a) 12-400-30-1, and b) 12-400-30-2.

3.2.3. Poles loaded at 60°

At this angle, two 9-400 and two 12-400 were subjected to a monotonically increasing load up to failure (i.e., the second loading regime). During loading, the first visible cracks appeared at loads of 201 and 142 kgF in 9-400-60-1 and 9-400-60-2, respectively. In 9-400-30-1 and 9-400-30-2, numerous flexural cracks developed in the flange at loads of 318 and 230 kgF, respectively, which subsequently propagated towards the web with increasing load. Finally, diagonal shear cracks occurred at the first two steps of the poles (inside the support) at a load of 600 kgF. The specimens 9-400-0-1 and 9-400-0-2 recorded maximum loading capacities of 1190 and 1205 kgF, respectively. The flexural and shear cracks in these two specimens are presented in Fig. 13.

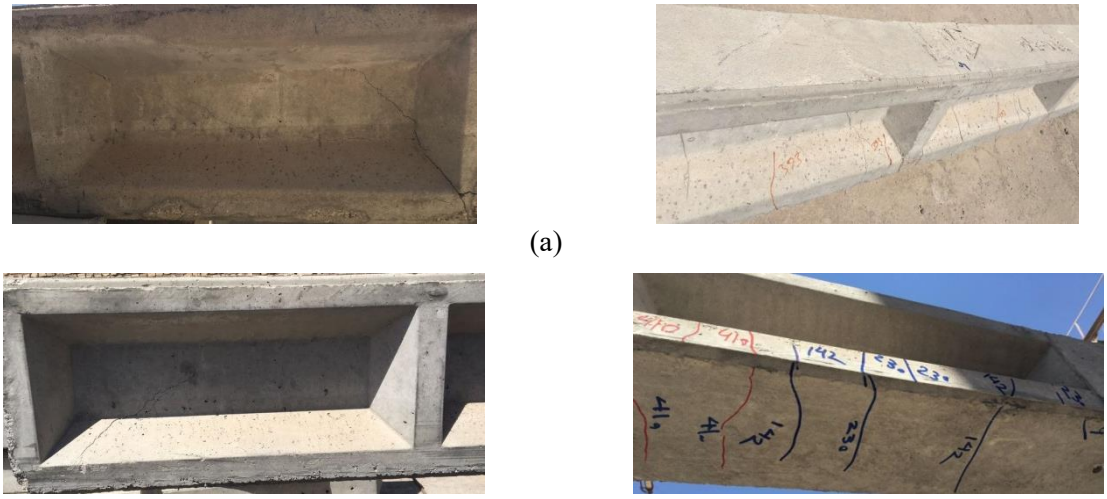

Fig. 13. Cracking in: a) 9-400-60-1, and b) 9-400-60-2.

Fig. 14 shows the shear and flexural cracks developed during loading in 12-400-60-1 and 12-400-60-2. The first cracks appeared in the tensile side at loads of around 180 kgF. Clearly, flexural cracks subsequently propagated towards the web. In the last loading stages, diagonal and flexural cracks appeared within the web inside the support leading to their ultimate failure. Finally, the poles failed at loads of 1026 and 1206 kgF, respectively. The failure mode in these specimens loaded at an angle of 60° occurred as a result of a combination of shear and flexural cracks.

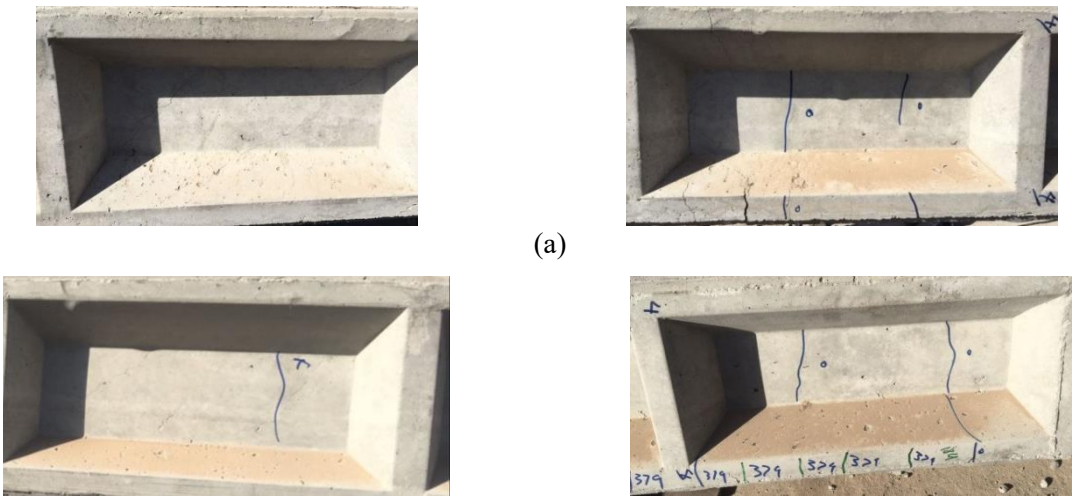

Fig. 14. Cracking patterns in: a) 12-400-60-1, and b) 12-400-60-2.

3.2.4. Poles loaded at 90°

The poles loaded at an angle of 90° were bent about their minor principal axes. Four poles, including two 9-400 and two 12-400 specimens, were tested at this angle under an incrementally increasing monotonic loading up to failure. Unlike the other directions, flexural behavior dominated the performance of the specimens loaded at this angle. The responses of 9-400-0-1 and 9-400-0-2 initiated with the formation of flexural cracks at loads of around 155 kgF followed by flexural cracks spreading along the poles as shown in Fig. 15. At loads of 405 and 301 kgF, flexural cracks propagated towards the web in 9-400-90-1 and 9-400-90-2, respectively. Eventually, the poles failed at loads of 1204 kgF for 9-400-90-1 and 1062 kgF for 9-400-90-2.

Flexural cracks in 12-400-90-1 and 12-400-90-2 initially formed at loads of 125 and 192 kgF,

respectively. As loading proceeded, the flexural behavior became more dominant. Finally, 12-400-90-1 and 12-400-90-2 failed at loads of 1056 and 1033 kgF, respectively. Fig. 16 shows the cracking patterns in these specimens.

(a)

(b)

Fig. 15. Cracking patterns in: a) 9-400-90-1, and b) 9-400-90-2.

(a)

(b)

Fig. 16. Cracking patterns in: a) 12-400-90-1, and b) 12-400-90-2.

3.3. Strain variations in reinforcement and concrete

Fig. 17 presents the strain variations in both the tensile reinforcement and compression concrete measured by the strain gauges installed about 300 mm away from the support towards the pole tip.

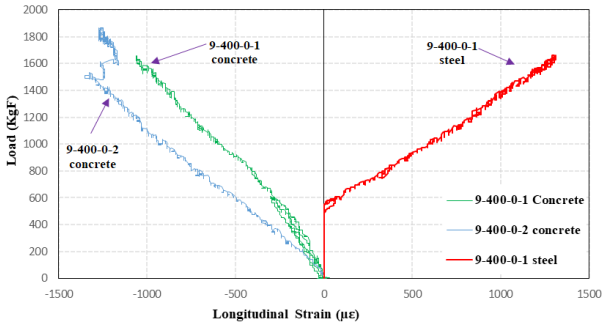

Fig. 17. Strain variations in steel rebars and concrete in 9-400-0-1 and 9-400-0-2.

It should be noted that the strain gauge installed on steel reinforcement in 9-400-0-2 failed during the fabrication and casting. The fluctuations in strain values versus the applied load were almost linear up to failure in both the steel rebars and concrete. The maximum tensile strain in steel rebars was 1300 με in 9-400-0-1, which is much lower than the yield strain (around 2000 με). Furthermore, maximum strain values in the compressive concrete in 9-400-0-1 and 9-400-0-2 varied between 1000 and 1400 με, which are lower than the strain corresponding to the maximum compressive strength of concrete (i.e., around 2000 με).

3.4. Stiffness

To compare the flexural stiffness of the tested poles, the concept of secant stiffness was used in this study. For each tested pole, the secant stiffness was defined as the slope of a line connecting the origin of coordinates to 75% the peak point ($0.75P_{max}$) [17]. Fig. 18 compares the flexural stiffness values obtained for all the tested poles. The highest flexural stiffness belonged to the specimens loaded at zero degree to bend about their major principal axes while those loaded at 90° to bend about their minor principal axes indicated the lowest stiffness.

3.5. Yield biaxial loading interaction diagram

The results obtained for the poles loaded at different directions were used to draw the relevant biaxial loading interaction curves shown in Fig. 19.

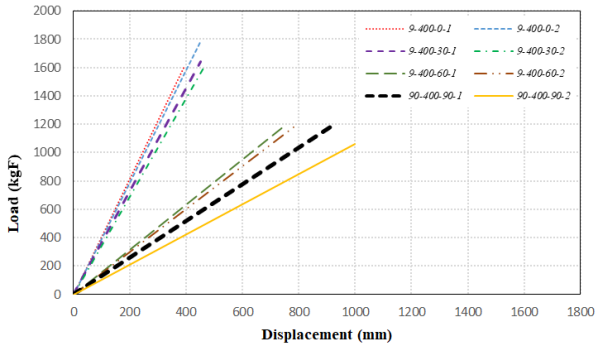

(a)

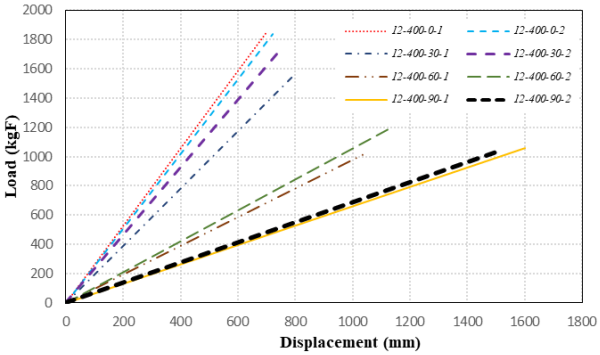

(b)

Fig. 18. Flexural stiffness in: a) 9-400, and b) 12-400 poles.

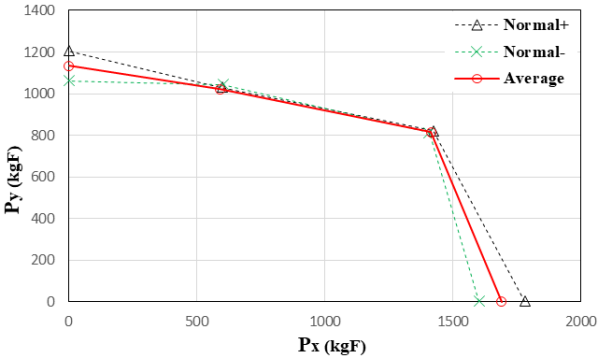

(a)

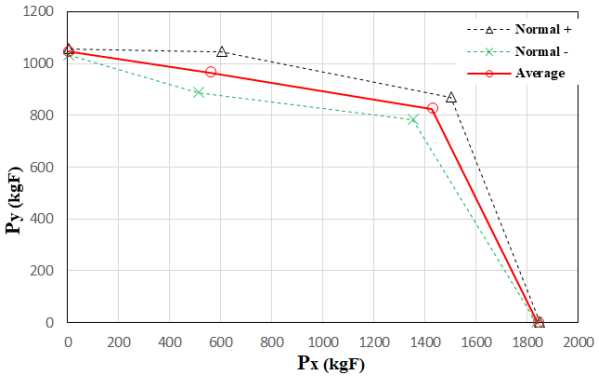

(b)

Fig. 19. Biaxial yield interaction diagrams for: a) 9-400 and, b) 12-400 poles.

The minimum and maximum load values were also marked with dashed lines. It should be noted that P_x and P_y are the biaxial loading capacity of the poles in X and Y directions, respectively (Fig. 2). These two diagrams may be exploited to predict the biaxial loading capacity of the 9-400 and 12-400 poles in any direction with a reliable accuracy.

4. Conclusions

The current study was conducted to elaborate on the structural performance of two commonly used H-type concrete poles (namely, 9-400 and 12-400) in four loading directions. To achieve this objective, a total number of sixteen concrete poles were fabricated and tested following the provisions stipulated by the Iranian Standard for H-type Utility Poles [15]. Based on the obtained results, the following conclusions may be drawn:

- Increasing the loading angle from zero to 90° led to a shift in the performance of poles from a shear failure to a purely flexural behavior.
- The loading capacity and stiffness of the concrete poles were declined with increasing loading angle while the ultimate displacement increased. The average resistance of the poles loaded at angles of 30, 60, and 90° relative to the minor principal axis was reduced by 3, 29, and 33.0% in 9-400 poles and by 11, 39, and 43% in 12-400 poles compared with those obtained for bending about their major principal axes.
- The ultimate loading capacity of the concrete poles when loaded to rotate about their major principal axes was found to be as high as four times their normal loading capacity.
- The setup proposed in the Iranian Standard for H-type Utility Poles [15] might lead to high shear forces exerted on the pole inside the support causing a shear failure when the pole is bend about its major principal axis. Such simulation is more conservative than the real field conditions. Hence, the loading capacity obtained from the experimental tests subjecting the poles to rotation about

their major axes is conservative. Thus, to strengthen the concrete poles, it is recommended to evaluate the possibilities of increasing their shear capacity at the support in future research studies.

References

[1] Kim J-K, Lee S-S. The behavior of reinforced concrete columns subjected to axial force and biaxial bending. Eng Struct 2000;22:1518–28. https://doi.org/10.1016/S0141-0296(99)00090-5.

[2] Ju Y, Zhao J, Wang D, Song Y. Experimental study on flexural behaviour of reinforced reactive powder concrete pole. Constr Build Mater 2021;312:125399. https://doi.org/10.1016/j.conbuildmat.2021.125399.

[3] Almutairi AD, Bai Y, Wang Y, Jeske J. Mechanical performance of fibre reinforced polymer confined softwood timber for pole applications. Compos Struct 2020;235:111807. https://doi.org/10.1016/j.compstruct.2019.111807.

[4] Saboori B, Khalili SMR. Static analysis of tapered FRP transmission poles using finite element method. Finite Elem Anal Des 2011;47:247–55. https://doi.org/10.1016/j.finel.2010.10.002.

[5] Rahnavard A, Yavartalab A, Samadi M, Zekavati A, Jafari MA. Development of seismic capacity curve (S.C.C.) for power distribution concrete poles. 22nd Int. Conf. Exhib. Electr. Distrib. (CIRED 2013), Institution of Engineering and Technology; 2013, p. 0406–0406. https://doi.org/10.1049/cp.2013.0714.

[6] Saberi H, Kolmi Zade V, Mokhtari A, Saberi V. Investigating of the effect of concrete confinement on the axial performance of circular concrete filled double-skin steel tubular (CFDST) long columns. J Rehabil Civ Eng 2020;8:43–59.

[7] Mahdavi N, Salimi M, Ghalehnovi M. Experimental study of octagonal steel columns filled with plain and fiber concrete under the influence of compressive axial load with eccentricity. J Rehabil Civ Eng 2021;9:1–18.

[8] Henin E, Morcous G, Tadros MK. Design, Fabrication, and Construction of Static-Cast Concrete Poles Reinforced with GFRP. Pract Period Struct Des Constr 2017;22. https://doi.org/10.1061/(ASCE)SC.1943-5576.0000333.

[9] Vivek B, Sharma S, Raychowdhury P, Ray-Chaudhri S. A study on failure mechanism of self-supported electric poles through full-scale field testing. Eng Fail Anal 2017;77:102–17. https://doi.org/10.1016/j.engfailanal.2016.12.019.

[10] Kliukas R, Daniunas A, Gribniak V, Lukoseviciene O, Vanagas E, Patapavicius A. Half a century of reinforced concrete electric poles maintenance: inspection, field-testing, and performance assessment. Struct Infrastruct Eng 2018;14:1221–32. https://doi.org/10.1080/15732479.2017.1402068.

[11] Kliukas R, Jaras A, Lukoševičienė O. Reinforced Spun Concrete Poles—Case Study of Using Chemical Admixtures. Materials (Basel) 2020;13:302. https://doi.org/10.3390/ma13020302.

[12] Argo M. Seismic Performance of Aging Prestressed Transmission Pole with Simulated Soil Foundation 2016.

[13] Baghmisheh AG, Mahsuli M. Seismic performance and fragility analysis of power distribution concrete poles. Soil Dyn Earthq Eng 2021;150:106909. https://doi.org/10.1016/j.soildyn.2021.106909.

[14] Zeynalian M, Khorasgani MZ. Structural performance of concrete poles used in electric power distribution network. Arch Civ Mech Eng 2018;18:863–76. https://doi.org/10.1016/j.acme.2018.01.005.

[15] Organization IEPD. Requirements of qualification tests for H-type reinforced concrete power distribution network poles 2020.

[16] International A. Specification for Deformed and Plain Carbon-Steel Bars for Concrete Reinforcement 2020. https://doi.org/10.1520/A0615_A0615M-20.

[17] Lai B, Liew JYR. Axial-moment interaction of high strength concrete encased steel composite columns: Experimental investigation. J Constr Steel Res 2020;175:106370. https://doi.org/10.1016/j.jcsr.2020.106370.